ACS APPLIED ELECTRONIC MATERIALS

pubs.acs.org/acsaelm

Article

Modification of Thermally Activated Delayed Fluorescence Emitters Comprising Acridan−Pyrimidine and Spiro-Acridan−Pyrimidine Moieties for Efficient Triplet Harvesting

Rita Butkute,* Steponas Raisys, Tomas Serevicius, Viktorija Andruleviciene, Aliyu Mahomed Hamisu, Gediminas Kreiza, Juozas V. Grazulevicius, and Saulius Jursenas

Cite This: https://doi.org/10.1021/acsaelm.4c02148

Read Online

ACCESS | Metrics & More | Article Recommendations | Supporting Information

ABSTRACT: In this study, we investigate the effect of substitution and conformational impact on the photophysical properties of novel 5-methylpyrimidine derivatives containing electron-donating groups with distinct rigidity. Research has revealed that all of the compounds showed pronounced thermally activated delayed fluorescence (TADF) features. The addition of the spiro-acridan moiety eliminated dual emission, simplifying the photophysical behavior of the compounds. Compounds containing spiro-acridan units exhibited a larger singlet−triplet energy gap, resulting in a reduced reverse intersystem crossing rate and an extended TADF lifetime in both toluene solutions and PMMA films. Additionally, the delayed fluorescence intensity was higher in these compounds, which was attributed to a slower nonradiative triplet quenching rate. Embedding TADF compounds into a rigid PMMA matrix significantly increases the quantum yield of delayed emission by minimizing nonradiative deactivation caused by intramolecular twisting. The considerable conformational disorder in the polymer-doped films leads to multiexponential fluorescence decay and noticeable shifts in both prompt and delayed fluorescence in time-resolved spectra. The attachment of electron-donating moieties at the fourth position in 5-methylpyrimidine reduces conformational disorder due to the restriction of the rotations caused by methyl attachment.

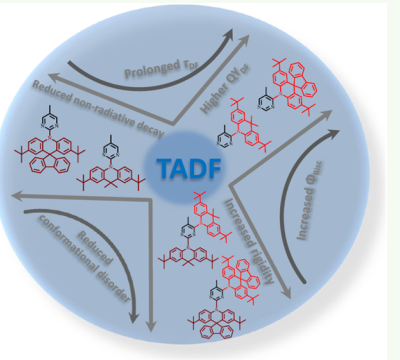

KEYWORDS: *pyrimidine, acridan, TADF, conformational disorder, rISC*

1. INTRODUCTION

Organic materials with the ability to efficiently harvest triplet excitons offer significant advantages for various applications, including OLED displays,[1] photodynamic therapy,[2] chemical sensors,[3] bioimaging,[4] etc. Thermally activated delayed fluorescence (TADF) is one of the most advanced strategies for utilizing triplet excitons.[5,6] TADF-based OLEDs can theoretically reach internal quantum efficiency (IQE) of unity by converting 75% of typically nonemissive triplet excitons through reverse intersystem crossing (rISC).[7] Achieving efficient TADF via rISC requires a very small singlet and triplet energy level splitting, which can be realized by designing compounds with spatially separated donor (D) and acceptor (A) units and arranged in an orthogonal fashion.[8] It has been shown that dynamical processes through lability between D and A facilitate the mixing of the lowest local-excitation triplet (^{3}LE) and the lowest charge transfer triplet (^{3}CT) states. This process enables significant second-order spin-vibronic coupling effects, increasing the rISC rate (k_{rISC}) by approximately 4 orders of magnitude and is therefore a key factor in determining TADF efficiency.[7,9]

The pyrimidine unit was selected as the acceptor core due to a weaker electron-accepting nature than the widely used triazine unit and hence can increase the band gap energy and S_1 and T_1 energy levels of TADF emitters. Therefore, the pyrimidine unit can serve as a universal building block for deep blue TADF materials. Moreover, the pyrimidine fragment can be easily substituted with various functional groups and the photophysical and electronic properties can be fine-tuned by simple chemical modifications.[10] Pyrimidine-based compounds adopting symmetrical configuration are promising TADF compounds, which attracted great interest among researchers for effective molecular design strategies.[11,12] Unlike symmetrical structures with two identical donor units, asymmetrical pyrimidine conformations typically link to a single donor, enabling more diverse substitutions with donors, acceptors, and the pyrimidine unit.[13] This makes their structure−property relationships appealing for further study.

Received: November 29, 2024
Revised: February 24, 2025
Accepted: February 28, 2025

Scheme 1. Structures and Synthesis of Pyrimidine Compounds[a]

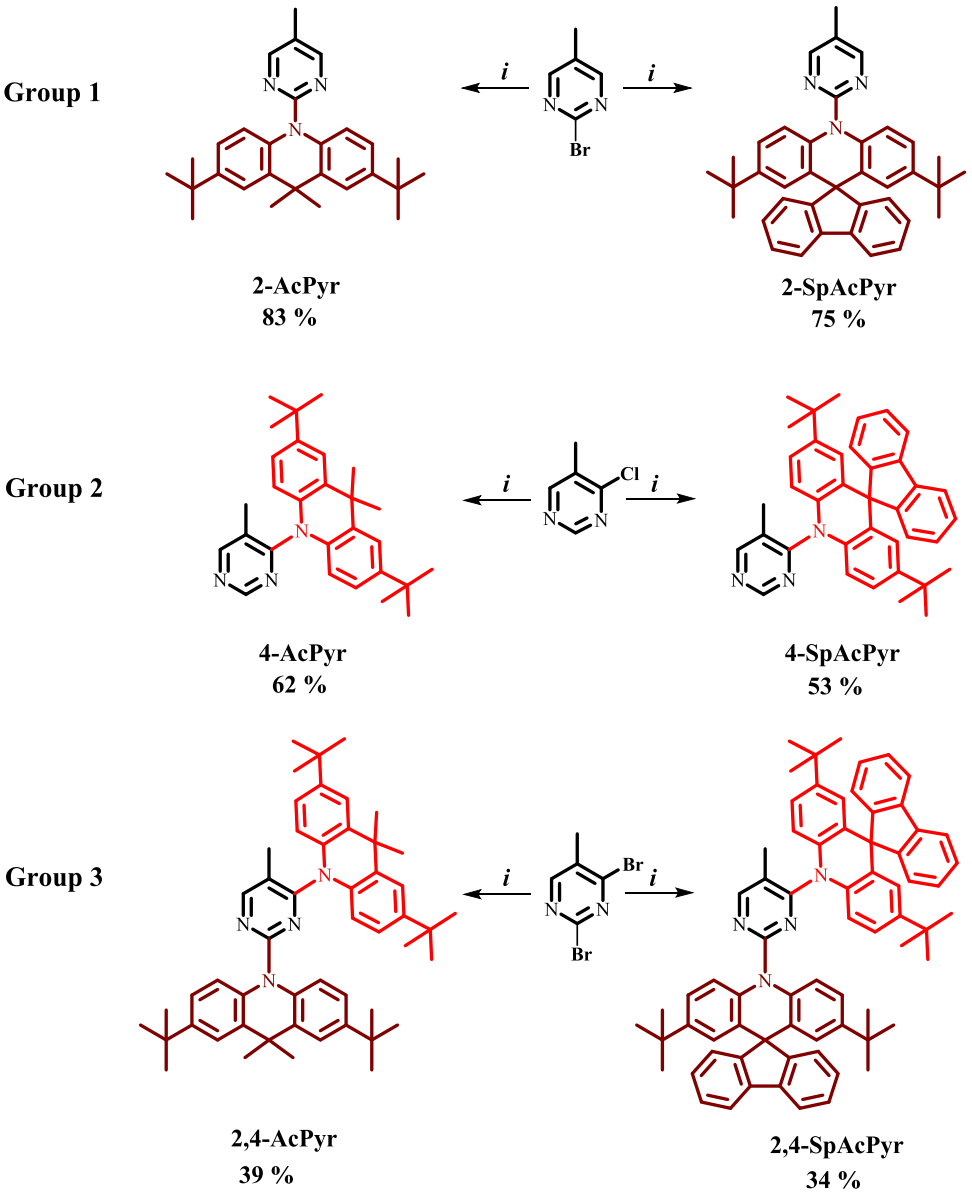

[a] *i* – 2,7-di-*tert*-butyl-9,9-dimethyl-9,10-dihydroacridine or 2,7-di-*tert*-butyl-10*H*-spiro[acridine-9,9′-fluorene], *t*-BuONa, Pd(*t*-Bu_3)$_2$, toluene, 110 °C.

9,9-Dimethyl-9,10-dihydroacridine is a key building block widely used in the development of TADF materials[14−16] due to its electron-rich nature, which enhances HOMO and LUMO separation. Moreover, its rigid structure helps to reduce nonradiative decay pathways from the excited state. However, in the presence of heteroatoms near the acridan fragment, central acridan ring forms a boat conformation, as previously published.[17−19] Since 9,9-dimethyl-9,10-dihydroacridine could adopt to a planar form and a bent form, a more rigid fragment, i.e., spiro-acridan, was frequently employed to enhance photoluminescence efficiency and avoid the dual emission.[1]

Building on the previous findings and aiming to understand better the connection between asymmetric D−A and D−A−D molecules, we design and investigate six isomeric D−A and D−A−D TADF emitters composed of 2,7-di-*tert*-butyl-9,9-dimethyl-9,10-dihydroacridine (DMAC) and 2,7-di-*tert*-butyl-10H-spiro[acridine-9,9′-fluorene] (SpAC) moieties attached at the 5-methylpyrimidine acceptor. Also, DMAC and SpAC units and the nature of their connection were chosen seeking a more pronounced alteration of TADF properties and a molecular rigidity increase.

2. EXPERIMENTAL METHODS

Thermogravimetric analysis (TGA) was performed using a TA Instruments TGA Q50 under a nitrogen atmosphere; samples were heated from 0 to 800 °C at a heating rate of 10 °C/min. Differential scanning calorimetry (DSC) was performed on TA Instruments DSC Q2000 series thermal analyzer. Heated rate was 10 °C/min.

Cyclic voltammetry (CV) measurements were obtained using a carbon working electrode in a three-electrode cell of an Autolab III potentiostat-galvanostat. The measurements were carried out for dry dichloromethane solutions containing 0.1 M tetrabutylammonium hexafluorophosphate at 25 °C. The scan rate was 50 mV/s while the sample concentration was 10^{-3} M. The potentials were measured against silver as a quasi-reference electrode. Platinum wire was used as

https://doi.org/10.1021/acsaelm.4c02148
ACS Appl. Electron. Mater. XXXX, XXX, XXX−XXX

Table 1. Thermal and Electrochemical Data of the Synthesized Compounds

compound	2-AcPyr	2-SpAcPyr	4-AcPyr	4-SpAcPyr	2,4-AcPyr	2,4-SpAcPyr
T_d, °C[a]	252	306	240	280	330	390
T_m, °C[b]	242	226	159	259	255	291
T_g, °C[c]	80	116	34	96	135	172
E_{ox}, V[d]	1.071	1.097	1.032	1.144	0.970	1.068
IP^{CV}, eV[e]	5.44	5.47	5.40	5.52	5.34	5.44
HOMO, eV[f]	−5.44	−5.48	−5.17	−5.14	−5.11	−5.11
LUMO, eV[f]	−1.00	−1.06	−1.39	−1.43	−1.26	−1.32

[a]Sublimation temperature established by TGA. [b]Melting temperature determined by DSC from the 1st heating scan. [c]Glass-transition temperature determined by DSC from the 2nd heating scan. [d]Oxidation potential vs Ag/Ag^+. [e]Ionization potential calculated according $IP^{CV} = (E_{ox} - E_{Fc/Fc^+}) + 4.8$. [f]Estimated from theoretical calculations (B3LYP/6-31G(d,p) level with CPCM in DCM).

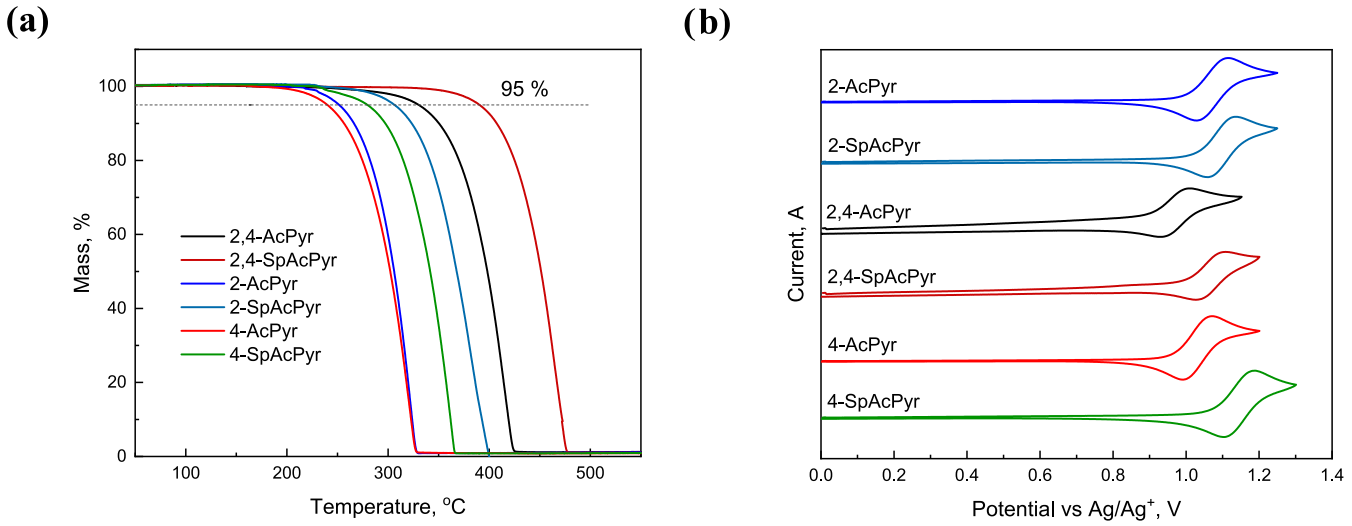

Figure 1. TGA curves (a) and CV voltammograms (b) (10^{-3} M dichloromethane solution, scan rate 50 mV/s, the potentials were measured against silver as a quasi-reference electrode).

the counter electrode. The potentials were calibrated with the standard ferrocene/ferrocenium (Fc/Fc^+) redox system.

Theoretical calculations were performed using density functional theory (DFT)[20] and with the B3LYP functional[21,22] at 6-31G(d,p) basis set level embedded in the Gaussian16 software.[23] The geometries of compounds were optimized in dichloromethane solution using the conductor-like polarizable continuum model (CPCM).

Solid-state films were prepared by a drop-casting method from tetrahydrofuran solutions. The THF stock solutions of each material and PMMA matrix were mixed at an appropriate ratio to give a desired concentration in the final films. Microscope cover glass slides were used as rigid protective substrates. The fabricated samples were encapsulated inside a nitrogen-filled glovebox using epoxy resin to seal the edges of the glass slides. The photophysical measurements were performed under ambient conditions. Toluene solutions were degassed using a freeze−pump−thaw method repeating five degassing cycles. The absorption spectra were measured using a Lambda 950 UV/vis spectrophotometer (PerkinElmer). Time-integrated and time-resolved fluorescence spectra, as well as low-temperature phosphorescence spectra and fluorescence transients, were measured using a time-gated iCCD camera New iStar DH340T (Andor), where nanosecond YAG:Nd^{3+} laser NT 242 (Ekspla, pulse width 7 ns, pulse energy 200 μJ, repetition rate 1 kHz) serves as an excitation source. Fluorescence quantum yields (Φ_{FL}, with ±5% error) of the solutions and films were evaluated by utilizing an integrating sphere (Sphere Optics) coupled to the CCD spectrometer PMA-12 (Hamamatsu) via an optical fiber.

Procedures of the synthesis of pyrimidine compounds and identification are described in the Supporting Information (Experimental Section).

3. RESULTS AND DISCUSSION

3.1. Molecular Design and Synthesis. 5-Methylpyrimidine was used as a basic scaffold, incorporating the electron-donating functions of DMAC and SpAC at various positions: the second, the fourth, and both the second and fourth positions. Initially, electron-donating moieties were attached at the second position of the 5-methylpyrimidine core (Group 1, Scheme 1). In this configuration, DMAC adopts a coplanar geometry with the pyrimidine core and exhibits a quasi-axial (QA) conformation (**2-AcPyr**). Substituting DMAC with a fluorene-modified SpAC moiety creates a more rigid fragment, preventing the QA conformation (**2-SpAcPyr**). Attaching the same electron-donating fragments at the fourth position alters the D−A angle due to the influence of the methyl group (compounds **4-AcPyr** and **4-SpAcPyr**, Group 2, Scheme 1). Combining the structures of Group 1 and Group 2 yields TADF compounds where the planar acridan moiety at the second position functions more as an acceptor, while the attachment at the fourth position serves as a donor (compounds **2,4-AcPyr** and **2,4-SpAcPyr**, Group 3, Scheme 1).

The synthesis involved a one-step Buchwald−Hartwig amination reaction of pyrimidine intermediates with corresponding donor molecules. This reaction was catalyzed by bis(tri*tert*-butyl-phosphine)palladium(0) using *t*-BuONa as a base (Scheme 1). 2,7-Di-*tert*-butyl-10*H*-spiro[acridine-9,9′-fluorene] was obtained using a direct cyclization reaction.[24] The structures of the synthesized compounds were verified by

https://doi.org/10.1021/acsaelm.4c02148
ACS Appl. Electron. Mater. XXXX, XXX, XXX−XXX

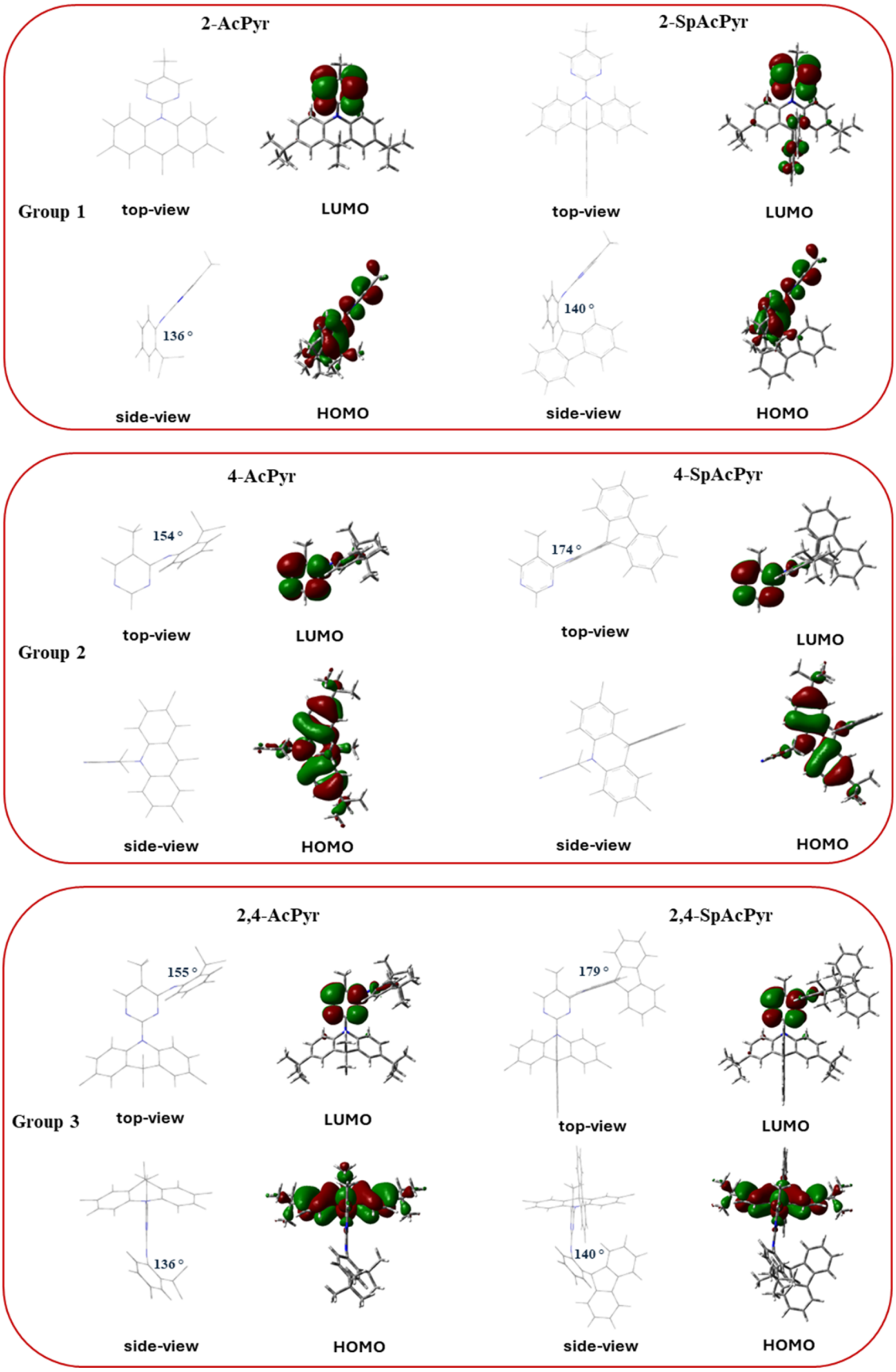

Figure 2. Theoretical geometries and frontier orbitals of pyrimidine-based compounds were obtained at the B3LYP/6-31G(d,p) level with CPCM in DCM (the alkyl groups in the top and side views of the structures have been removed to make the geometries of the compounds more clearly visible).

https://doi.org/10.1021/acsaelm.4c02148
ACS Appl. Electron. Mater. XXXX, XXX, XXX−XXX

^{1}H NMR, ^{13}C NMR, mass spectrometry, and elemental analysis (see Figures S1−S18). Detailed synthetic procedures for pyrimidines and their product characterization are provided in the Supporting Information.

3.2. Thermal and Electrochemical Characteristics. The thermal properties of the final compounds were evaluated by thermogravimetric analysis (TGA) and differential scanning calorimetry (DSC), and the results and the data are provided in Table 1 and Figures 1a and S19.

All compounds demonstrate high thermal stability (T_d, corresponding to 5% weight loss) in the range from 240 to 390 °C (Figure 1a). During TGA measurements, complete weight loss of compounds was observed, indicating sublimation of the compounds. The DSC curves reveal the glass-forming abilities of all compounds. Second heating scans show that these pyrimidine compounds, except **2-AcPyr**, can be transformed into a stable amorphous state (Figure S19) with the glass-transition temperatures (T_g) ranging from 34 to 172 °C. The introduction of SpAC increases values of sublimation and glass-transition temperatures compared with the introduction of DMAC. Compounds having substituents at the fourth pyrimidine position have lower glass-transition and sublimation temperatures than compounds having substituents in the second position due to a more constrained structure because of methyl substituent.

The different conformations of DMAC and SpAC moieties impair the electron-donating ability of these groups, as demonstrated by subsequent CV tests, shown in Figure 1b. The oxidation waves of **2-AcPyr** and **2-SpAcPyr** almost begin at the same position due to their similar molecular geometry with respect to the pyrimidine core. Their IP^{CV} values were calculated to be 5.44 and 5.47 eV, respectively. More differences can be seen when electron-donating moieties are near the methyl group in the pyrimidine structure (**4-AcPyr**, **4-SpAcPyr**, **2,4-AcPyr**, and **2,4-SpAcPyr**). In that case, IP^{CV} values for compounds containing more rigid SpAC moieties are higher compared with those for DMAC-containing compounds due to reduced electron-donating ability. During the positive potential sweep, all compounds exhibited reversible oxidation peaks. Additionally, it was observed that the electrochemical peak values remained consistent across repeated cycles, indicating the formation of stable cations. No reduction waves were observed within the electrochemical window during the negative potential sweep, highlighting the weak electron-accepting character of the pyrimidine core. DFT calculations showed that the HOMO energies of the synthesized compounds range from −5.11 to −5.48 eV, while the LUMO energies range from −1.00 to −1.43 eV.

These pyrimidine compounds exhibit thermal and electrochemical properties that make them attractive for applications in optoelectronic devices.

3.3. Geometries and Frontier Orbitals. The X-ray geometries of **2,4-AcPyr** and **2,4-SpAcPyr** presented in Figure S20 revealed that DMAC moieties in **2,4-AcPyr** obtain bent geometry (136° and 144°) are in quasi-axial and somewhat quasi-equatorial configuration at the second and fourth positions of 5-methylpyrimidine ring, respectively. After the introduction of fluorene units in a spiro configuration (**2,4-SpAcPyr**), the SpAC moiety at the second position of the 5-methylpyrimidine retains its bent geometry (139°) and quasi-axial configuration. In contrast, SpAC at the fourth position undergoes significant planarization (up to 167°) and adopts a strong quasi-equatorial orientation, forming a dihedral angle of 84°. The X-ray and theoretical geometries of **2,4-AcPyr** and **2,4-SpAcPyr** (Figures 2 and S20) exhibit a similar global shape. The differences in geometries arise because of the crystal-packing forces, which are absent during the theoretical geometry optimization of the isolated molecules. Similar observations were made for the theoretical geometries of **2-AcPyr**, **2-SpAcPyr**, **4-AcPyr**, and **4-SpAcPyr** having one DMAC or SpAC moiety attached only at the second or fourth position of the 5-methylpyrimidine ring (Figure 2). As a result, the HOMO for **4-AcPyr**, **4-SpAcPyr**, **2,4-AcPyr**, and **2,4-SpAcPyr** is localized on the di-*tert*-butyl-acridan moiety, which adopts a quasi-equatorial conformation (fourth position). This occurs because the methyl group in ortho-position relative to the electron-donating fragment helps to maintain the twist angles between D and A, thereby increasing the separation of the orbitals. In contrast, the quasi-axial configuration of the acridan moiety in **2-AcPyr** and **2-SpAcPyr** causes the HOMO distribution across the di-*tert*-butyl-acridan and 5-methylpyrimidine fragments. In all compounds, LUMO is located mainly on the 5-methylpyrimidine core.

3.4. Absorption and Emission Properties. The absorption and fluorescence spectra of pyrimidine compounds were analyzed in dilute toluene solutions and polymer films. The spectral data are depicted in Figure 3 and summarized in Table 2.

As seen in Figure 3, the weaker absorption spanning the 325−450 nm range for compounds **4-AcPyr**, **4-SpAcPyr**, **2,4-AcPyr**, and **2,4-SpAcPyr** and 325−375 nm range for compounds **2-AcPyr** and **2-SpAcPyr** is assigned to the intramolecular charge transfer (ICT) transitions, primarily from the electron-rich DMAC or SpAC to the electron-deficient pyrimidine unit. The lowest molar absorption coefficient (ε) was observed for **4-AcPyr** and **4-SpAcPyr** (ε = 1200 and 1000 $M^{-1}cm^{-1}$, respectively). In contrast, compounds **2,4-AcPyr** and **2,4-SpAcPyr** exhibited the highest ε, approximately 4800 and 2300 M^{-1} cm^{-1}.

The fluorescence spectra of toluene solutions exhibit emission peaks in the region of 471−527 nm (Figure 3). When embedded in a solid poly(methyl methacrylate) (PMMA) matrix at 1 wt % doping concentration, the emission spectra of all compounds have shifted to the blue region. Such blue shift may arise from the lower polarity of the polymer surrounding as well as the conformational distribution of the D−A twist angle, inducing the broadening of the emission spectrum.[25]

The fluorescence and phosphorescence (PH) spectral measurements at low temperatures allowed for the experimental determination of singlet−triplet energy splitting ($\Delta E_{S_1T_1}$). As shown in Table 2 and Figure S21, $\Delta E_{S_1T_1}$ for compounds with SpAC moieties was higher, while for compounds with DMAC moieties, ΔE_{S1T1} is relatively low. The estimated $\Delta E_{S_1T_1}$ values were in the region from 101 to 477 meV. The substitution of the acridan unit with fluorene had an evident impact on the line shape of phosphorescence spectra (Figure 3). For **2-AcPyr**, **4-AcPyr**, and **2,4-AcPyr**, PH spectra were structureless, while for **2-SpAcPyr**, **4-SpAcPyr**, and **2,4-SpAcPyr**, a clear vibronic pattern was observed. As DFT calculations and XRD analysis revealed, the introduction of fluorene moiety transforms acridan from axial to equatorial orientation and increases its twist angle. This structural modification then transforms structureless PH, suffering from

https://doi.org/10.1021/acsaelm.4c02148
ACS Appl. Electron. Mater. XXXX, XXX, XXX−XXX

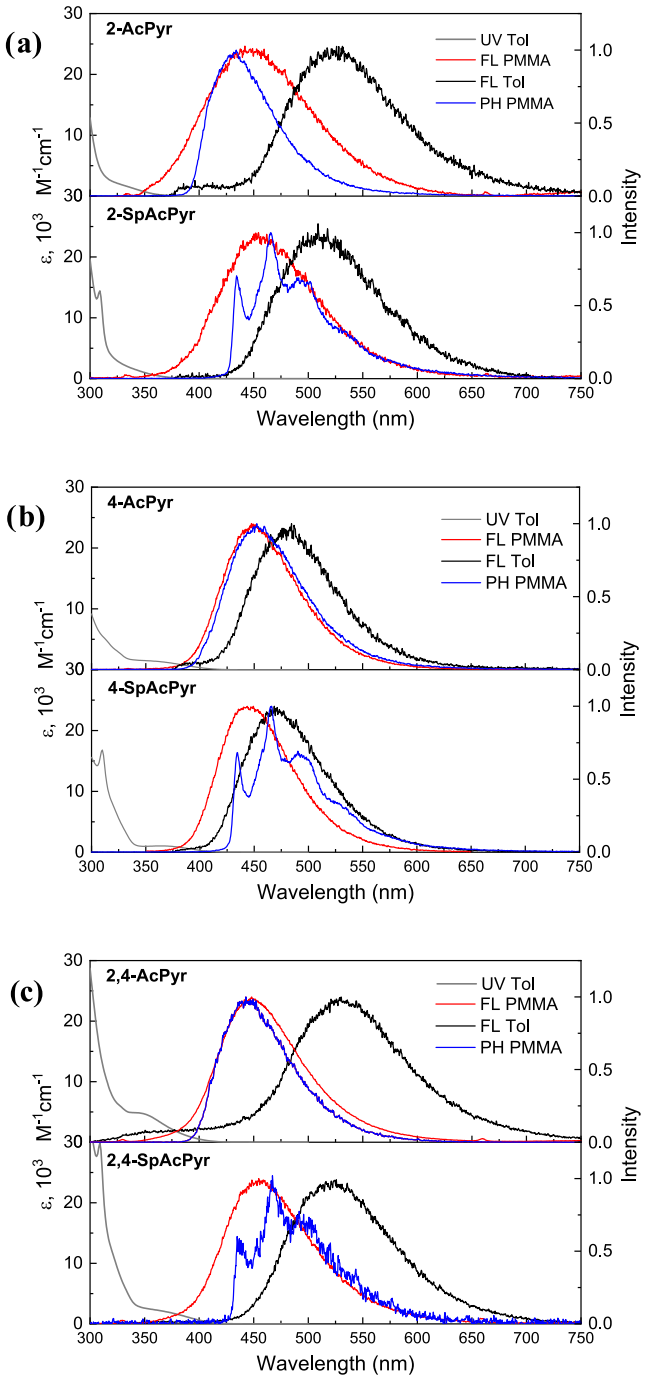

Figure 3. Absorption of toluene solutions (gray lines), fluorescence of 1 wt % PMMA films (red lines) and toluene solutions (black lines), and phosphorescence of 1 wt % PMMA film (blue lines) spectra of compounds **2-AcPyr** and **2-SpAcPyr** (a), **4-AcPyr** and **4-SpAcPyr** (b), and **2,4-AcPyr** and **2,4-SpAcPyr** (c).

structural relaxations in the excited state, to that having a clear pattern, typical of the local-excitation character emission.

Electron-donating DMAC moiety joined at the second position between the heteroatoms (**2-AcPyr**) sits in a coplanar geometry and is characterized by QA conformation. Compound **2-AcPyr** exhibited dual ICT fluorescence of a toluene solution (Figure 3a). Dual emission was not observed in the toluene solution of compound **2-SpAcPyr**, containing a SpAC moiety, due to the planarized conformation of the acridan part in the SpAC structure. Flattering of acridan using spiro-fluorene showed a slightly blue-shifted emission due to lowered conjugation and lowered nonradiative (k_{nr}^{T}) decay rate (Table 3). Embedding in a solid PMMA matrix reduces the nonradiative decay due to space constraints, which results in a slight PLQY increase.

DMAC moiety joined at the fourth position next to the methyl substituent (**4-AcPyr**) has a perpendicular dihedral angle between the D−A parts and, therefore, is less conjugate. In this case, flattering of acridan works in the opposite way. Attachment of fluorene reduces the nonradiative decay rate of toluene solution, which results in changes in the photoluminescence quantum yield of delayed fluorescence (Φ_{DF}) from 0.10 to 0.31 for compounds **4-AcPyr** and **4-SpAcPyr**, respectively. After embedding in rigid PMMA matrix, flattering of acridan has no influence because the rotation of the acridan fragment is already restricted by the methyl substituent. Therefore, Φ_{DF} does not change and is equal for both compounds (Table 2).

Combining these two groups of structures (Group 3, Scheme 1) allows us to understand how the donor fragments act in the combined D−A−D system. In this case, we have one electron-donating moiety (D1) attached between heteroatoms and another one (D2) near the methyl group. Compound **2,4-AcPyr** exhibited dual ICT fluorescence in toluene solution (Figure 3c) of QA conformation of D1 and ordinary ICT nature. As in the case of compound **2-SpAcPyr**, dual emission is not observed for compound **2,4-SpAcPyr**, containing SpAC moiety instead of DMAC. D1 and D2 have different effects, according to the information obtained from the analysis of Group 1 and Group 2 compounds. A slight red shift in the case of the PMMA film of compound **2,4-SpAcPyr** is visible due to the different conjugation of D1 and D2 fragments (Figure 3c). A relatively similar k_{FL} of toluene solutions was observed for compounds **2,4-AcPyr** and **2,4-SpAcPyr**. The low Φ_{FL} values of the toluene solutions (0.02 and 0.04 for **2,4-AcPyr** and **2,4-SpAcPyr**, respectively) increase after the dispersion of the compounds in the PMMA matrix due to a decrease in the nonradiative decay rate, reaching 0.44 and 0.42, respectively.

3.5. TADF Properties. Further investigation of pyrimidine compounds was carried out by analyzing the time-resolved emission properties. The calculated TADF parameters for toluene solutions of the compounds are listed in Table 3. The delayed fluorescence, observed exclusively for all compounds, was identified as TADF. The increase of fluorescence lifetime of compounds was enhanced after oxygen removal from toluene solutions (Figure S22).

In the case of compounds with substituents at the second position of the pyrimidine core (Group 1), where the rotation of the substituents is not restricted, the flattering of acridan moiety (**2-SpAcPyr**) results in an increase of intensity of delayed fluorescence (DF) comparing with compound **2-AcPyr** (Table 3). The lowering of the rISC rate due to the increase in $\Delta E_{S_1T_1}$ after the introduction of fluorene units in spiro configuration is visible; therefore, the lifetime of DF increases.

Similar trends were observed for compounds **4-AcPyr** and **4-SpAcPyr** (Group 2). As shown in Figure 4b and Table 3, the introduction of the SpAc moiety at the fourth position of the pyrimidine core has a significant impact on TADF properties and lowers the rISC rate and prolongs the DF lifetime in toluene solutions as well as enhances rISC efficiency by lowering the nonradiative triplet decay rate. However, the rISC

https://doi.org/10.1021/acsaelm.4c02148
ACS Appl. Electron. Mater. XXXX, XXX, XXX−XXX

Table 2. Photophysical Properties of Pyrimidine Compounds under the O_2-Deficient Conditions of Toluene Solutions and PMMA Films

	toluene[a]					PMMA[b]					
	λ_{ABS}, nm	ε, M^{-1} cm^{-1}	λ_{PL}, nm	Φ_{PF}/Φ_{DF}	$k_{FL}/k_r/k_{nr}^S$, 10^7 s^{-1}[c]	λ_{PL}, nm	Φ_{PF}/Φ_{DF}	$k_{FL}/k_r/k_{nr}^S$, 10^7 s^{-1}	S_1, eV[d]	T_1, eV[d]	$\Delta E_{S_1T_1}$, meV[d]
2-AcPyr	328	1900	522	0.01/0.02	8.5/0.1/8.4	453	0.03/0.08	6.3/0.2/6.1	3.32	3.16	163
2-SpAcPyr	331	2300	500	0.01/0.01	5.4/0.1/5.3	468	0.04/0.10	4.4/0.2/4.2	3.33	2.85	477
4-AcPyr	368	1200	481	0.02/0.10	2.8/0.1/2.7	460	0.09/0.40	4.1/0.4/3.7	3.20	3.10	101
4-SpAcPyr	363	1000	471	0.05/0.31	3.5/0.2/3.3	451	0.06/0.40	5.3/0.3/5.0	3.16	2.86	302
2,4-AcPyr	347	4800	527	0.01/0.01	7.2/0.1/7.1	448	0.06/0.38	7.8/0.5/7.3	3.31	3.12	196
2,4-SpAcPyr	360	2300	515	0.02/0.02	5.5/0.1/5.4	457	0.05/0.37	6.4/0.3/6.1	3.15	2.87	276

[a]Determined in degassed toluene solutions (10^{-5} M). [b]PMMA films (1 wt %) under oxygen-free environment. [c]Rate constants of fluorescence $k_{FL} = 1/\tau_{PF}$; radiative decay rate of fluorescence $k_r = \phi_{PF}/\tau_{PF}$; nonradiative decay rate of fluorescence $k_{nr}^S = k_{FL}\cdot(1 - \phi_{PF})$. [d]Estimated from the onset of fluorescence and phosphorescence spectra at 10 K.

Table 3. Photophysical Properties of Pyrimidine Compounds under the O_2-Deficient Conditions in Toluene Solutions[a,b,c,d,e]

	Φ_{FL}[e]	τ_{PF}, ns[e]	τ_{DF}, μs[e]	DF/PF	Φ_{ISC}	Φ_{rISC}	k_{ISC}, 10^6 s^{-1}[e]	k_{rISC}, 10^6 s^{-1}[e]	k_{nr}^T, 10^6 s^{-1}[e]
2-AcPyr	0.03/0.01/0.02	11.8	0.42	2.0	0.99	0.67	83.9	5.57	2.41
2-SpAcPyr	0.02/0.01/0.01	18.7	1.33	1.0	0.99	0.51	53.0	0.43	0.76
4-AcPyr	0.12/0.02/0.10	35.8	1.23	5.0	0.98	0.85	27.4	4.04	0.90
4-SpAcPyr	0.36/0.05/0.31	28.8	9.40	6.2	0.95	0.91	33.0	0.63	0.14
2,4-AcPyr	0.02/0.01/0.01	14.0	0.40	1.0	0.99	0.51	70.7	1.71	2.55
2,4-SpAcPyr	0.04/0.02/0.02	18.3	0.54	1.0	0.98	0.51	53.5	1.80	1.90

Parameters were assessed according to Kreiza et al.[26] [a]Fluorescence quantum yield of total, prompt, and delayed fluorescence, respectively. [b]Prompt and delayed fluorescence decay time. [c]Intersystem crossing rate, $k_{ISC} = \Phi_{ISC}/\tau_{PF}$, $\Phi_{ISC} = (1 - \Phi_{PF})$. [d]Reverse intersystem crossing rate, $k_{rISC} = \Phi_{rISC}/\tau_{DF}\cdot((\Phi_{PF} + \Phi_{DF})/\Phi_{PF})$, $\Phi_{rISC} = \Phi_{DF}/((\Phi_{DF} + \Phi_{PF})\cdot\Phi_{ISC})$. [e]Nonradiative triplet quenching rate, $k_{nr}^T = k_{rISC}/\Phi_{rISC} - k_{rISC}$.

rate was larger for **2,4-AcPyr** and **2,4-SpAcPyr** (1.71×10^6 and 1.80×10^6 s^{-1}) compared with **4-SpAcPyr** (6.31×10^5 s^{-1}), due to the lower singlet−triplet gap. While the TADF parameters were similar for compounds **2,4-AcPyr** and **2,4-SpAcPyr**, the DF intensity was higher for compound **2,4-SpAcPyr** due to the slower k_{nr}^T (Table 3 and Figure 4c).

An increase in Φ_{DF} was achieved by embedding compounds in the PMMA matrix. Both prompt and delayed fluorescence exhibited a multiexponential decay profile due to conformational disorder (CD) in compounds (Figure 4), making it difficult to estimate decay constants accurately.

Time-resolved fluorescence spectra (TRFS) were recorded for 1 wt % PMMA films to assess the conformational disorder in pyrimidine-based TADF compounds (Figure 5). The rigid PMMA matrix trapped TADF molecules in various configurations with twist angles between donor and acceptor units dispersed in a wide range. Configurations, those with larger $\Delta E_{S_1T_1}$, exhibited higher oscillator strength, and therefore emitted light first, while smaller $\Delta E_{S_1T_1}$ resulted in weaker oscillator strength and slower decay. Therefore, a red shift in the initial prompt emission over time before the system decayed into the triplet manifold was observed. At later times, molecules with smaller $\Delta E_{S_1T_1}$ emitted first while those with the larger $\Delta E_{S_1T_1}$ and accordingly higher S_1 energy emitted last blue-shifting the emission spectrum.

The nature of the substitution of the pyrimidine compounds influences the conformational disorder. As depicted in Figures 5 and S23, the red shift in the temporal emission closely matches the blue shift observed for pyrimidine compounds. The biggest change in TRFS is visible for compounds having DMAC and SpAC moieties at the second position of the pyrimidine core. The attachment of DMAC and SpAC moieties at the fourth position at 5-methylpyrimidine reduces conformational disorder as observed in TRFS. In the case of disubstituted compounds (**2,4-AcPyr** and **2,4-SpAcPyr**), shifts of spectra in TRFS are smaller due to the restriction of the rotations of one of the fragments attached at the fourth position by the methyl group. CD for compounds **4-AcPyr** and **4-SpAcPyr** is minor compared with other compounds due to the most constrained structure. In TRFS of compounds having electron-donating moieties at the second or the second and fourth positions, a decrease in the fluorescence intensity of the QA conformer is evident, confirming that the dual fluorescence involves ordinary fluorescence (QA) and TADF (QE). More intense emission of the QA conformers is observed in the case of compounds with DMAC substituents, which again proves that the acridan moiety is more planar in the spiro form with fluorene.

In general, the temporal dynamics of compounds depend on the structure and substituents that restrict donor−acceptor rotations, which promote differences in conformational disorder.[27]

4. CONCLUSIONS

This study demonstrates the effects of substitution and conformational properties on the photophysical behavior of novel 5-methylpyrimidine derivatives with electron-donating groups of varying rigidity. All compounds exhibited pronounced thermally activated delayed fluorescence (TADF) characteristics. Adding a spiro-acridan moiety eliminated dual emission, simplifying the photophysical behavior of the compounds. Compounds with spiro-acridan units demonstrated a larger singlet−triplet energy gap, leading to a reduced reverse intersystem crossing (rISC) rate and an extended TADF lifetime in both toluene solutions and PMMA films. Higher delayed fluorescence intensity in spiro-acridan compounds was attributed to slower nonradiative triplet

https://doi.org/10.1021/acsaelm.4c02148
ACS Appl. Electron. Mater. XXXX, XXX, XXX−XXX

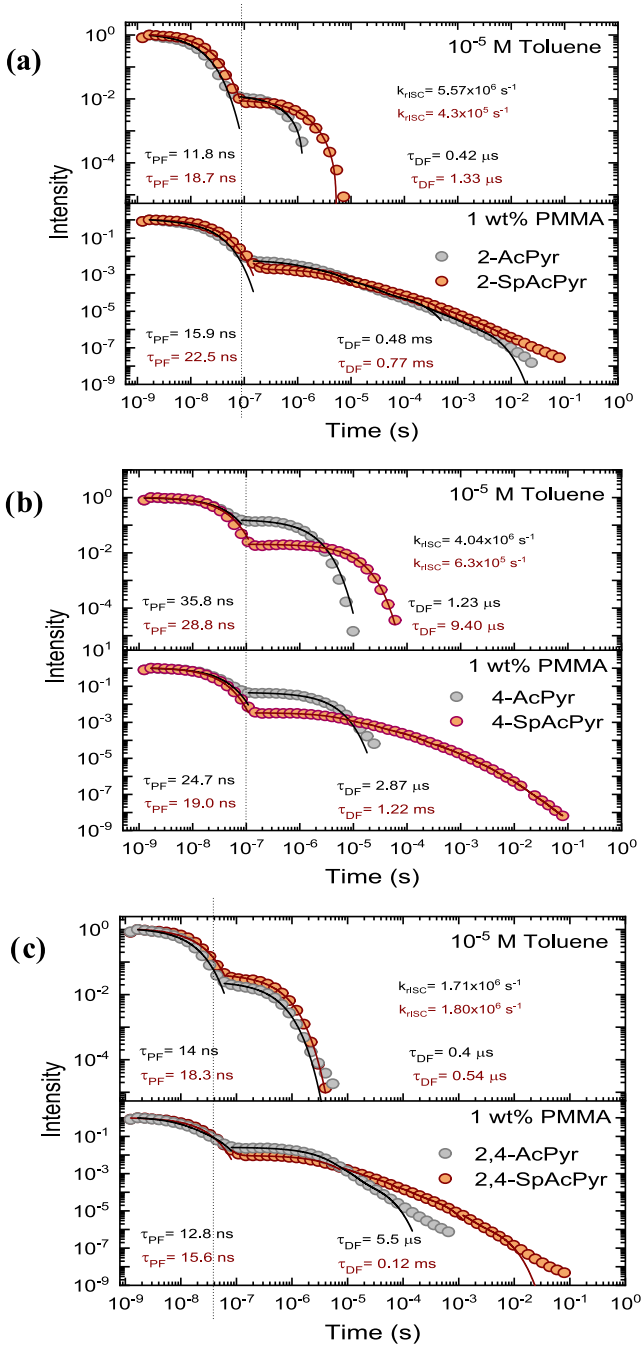

Figure 4. Normalized photoluminescence decay transients of compounds **2-AcPyr** and **2-SpAcPyr** (a), **4-AcPyr** and **4-SpAcPyr** (b), and **2,4-AcPyr** and **2,4-SpAcPyr** (c) of toluene solutions and 1 wt % PMMA films under oxygen-free conditions. Thin color lines represent exponential fits.

quenching rates. Embedding TADF compounds in a rigid PMMA matrix significantly enhanced the quantum yield of delayed emission by reducing nonradiative pathways associated with intramolecular twisting. Polymer-doped films exhibited notable conformational disorder, resulting in nonexponential fluorescence decay and shifts in prompt and delayed fluorescence in time-resolved spectra. Introducing electron-donating moieties at the fourth position of 5-methylpyrimidine reduced conformational disorder by restricting rotational flexibility, highlighting the role of structural modifications in optimizing photophysical properties.

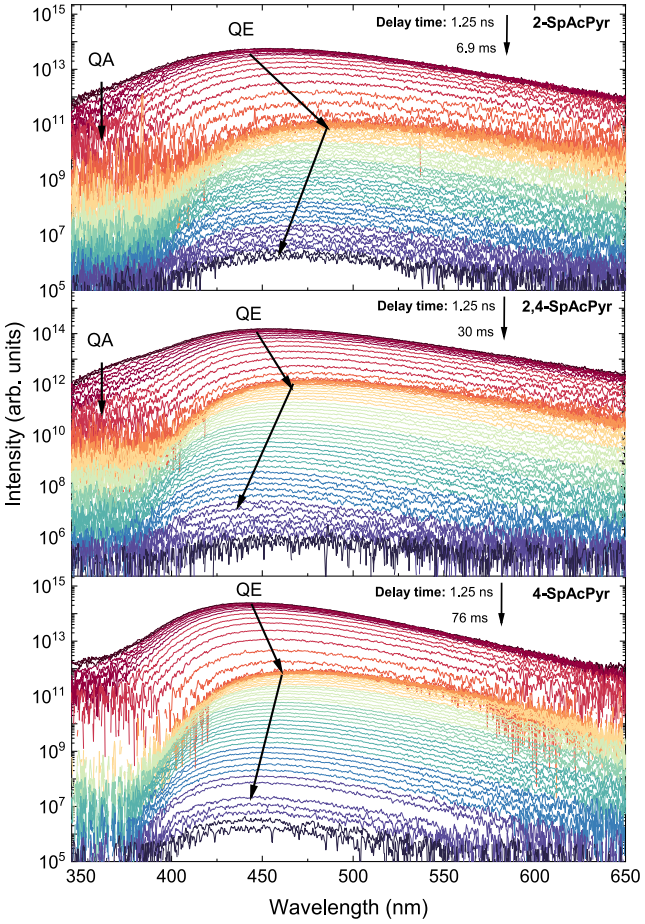

Figure 5. Time-resolved fluorescence spectra of 1 wt % PMMA films of compounds **2-SpAcPyr**, **2,4-SpAcPyr**, and **4-SpAcPyr** under O_2-deficient conditions. The initial and latest delay times are also shown.

■ ASSOCIATED CONTENT

Supporting Information

The Supporting Information is available free of charge at https://pubs.acs.org/doi/10.1021/acsaelm.4c02148.

Copies of NMR spectra, detailed descriptions of the synthesis and identification, general experimental information, DSC curves, and additional photophysical data. (PDF)

■ AUTHOR INFORMATION

Corresponding Author

Rita Butkute − *Institute of Photonics and Nanotechnology, Vilnius University, LT-10257 Vilnius, Lithuania; Department of Polymer Chemistry and Technology, Kaunas University of Technology, LT-51423 Kaunas, Lithuania;* orcid.org/0000-0001-6655-4565; Email: rita.butkute@ktu.lt

Authors

Steponas Raisys − *Institute of Photonics and Nanotechnology, Vilnius University, LT-10257 Vilnius, Lithuania;* orcid.org/0000-0002-5810-7199

Tomas Serevicius − *Institute of Photonics and Nanotechnology, Vilnius University, LT-10257 Vilnius, Lithuania;* orcid.org/0000-0003-1319-7669

https://doi.org/10.1021/acsaelm.4c02148
ACS Appl. Electron. Mater. XXXX, XXX, XXX−XXX

Viktorija Andruleviciene − *Department of Polymer Chemistry and Technology, Kaunas University of Technology, LT-51423 Kaunas, Lithuania*

Aliyu Mahomed Hamisu − *Department of Polymer Chemistry and Technology, Kaunas University of Technology, LT-51423 Kaunas, Lithuania*

Gediminas Kreiza − *Institute of Photonics and Nanotechnology, Vilnius University, LT-10257 Vilnius, Lithuania;* orcid.org/0000-0002-6992-1620

Juozas V. Grazulevicius − *Department of Polymer Chemistry and Technology, Kaunas University of Technology, LT-51423 Kaunas, Lithuania;* orcid.org/0000-0002-4408-9727

Saulius Jursenas − *Institute of Photonics and Nanotechnology, Vilnius University, LT-10257 Vilnius, Lithuania*

Complete contact information is available at: https://pubs.acs.org/10.1021/acsaelm.4c02148

Author Contributions

R.B., T.S., and S.J. designed the research. R.B. and H.A.M. performed synthesis, R.B. and S.R. were responsible for the photophysical studies, R.B. was responsible for thermal analyses and electrochemical investigations, and V.A. performed DFT calculations. G.K. was responsible for XRD analysis. R.B., T.S., J.V.G., and S.J. wrote the manuscript with support and contributions from all authors.

Notes

The authors declare no competing financial interest.

■ ACKNOWLEDGMENTS

This project has received funding from the Research Council of Lithuania (LMTLT), Agreement No. S-PD-22-83. S.R., T.S., G.K., and S.J. acknowledge the "Universities' Excellence Initiative" program by the Ministry of Education, Science and Sports of the Republic of Lithuania under the agreement with the Research Council of Lithuania (Project No. S-A-UEI-23-6).

■ REFERENCES

(1) Lim, H.; Cheon, H. J.; Woo, S.-J.; Kwon, S.-K.; Kim, Y.-H.; Kim, J.-J. Highly Efficient Deep-Blue OLEDs using a TADF Emitter with a Narrow Emission Spectrum and High Horizontal Emitting Dipole Ratio. *Adv. Mater.* **2020**, *32*, No. 2004083.

(2) Nguyen, V.-N.; Yan, Y.; Zhao, J.; Yoon, J. Heavy-atom-free photosensitizers: from molecular design to applications in the photodynamic therapy of cancer. *Acc. Chem. Res.* **2021**, *54*, 207.

(3) Zhou, Y.; Qin, W.; Du, C.; Gao, H.; Zhu, F.; Liang, G. Long-Lived Room-Temperature Phosphorescence for Visual and Quantitative Detection of Oxygen. *Angew. Chem., Int. Ed.* **2019**, *131*, 12230.

(4) Zhou, W.-L.; Lin, W.; Chen, Y.; Liu, Y. Supramolecular assembly confined purely organic room temperature phosphorescence and its biological imaging. *Chem. Sci.* **2022**, *13*, 7976.

(5) Uoyama, H.; Goushi, K.; Shizu, K.; Nomura, H.; Adachi, C. Highly efficient organic light-emitting diodes from delayed fluorescence. *Nature* **2012**, *492*, 234.

(6) Dos Santos, J. M.; Hall, D.; Basumatary, B.; Bryden, M.; Chen, D.; Choudhary, P.; Comerford, T.; Crovini, E.; Danos, A.; De, J.; Diesing, S.; Fatahi, M.; Griffin, M.; Kumar Gupta, A.; Hafeez, H.; Hämmerling, L.; Hanover, E.; Haug, J.; Heil, T.; Karthik, D.; Kumar, S.; Lee, O.; Li, H.; Lucas, F.; Mackenzie, C. F. R.; Mariko, A.; Matulaitis, T.; Millward, F.; Olivier, Y.; Qi, Q.; Samuel, I. D. W.; Sharma, N.; Si, C.; Spierling, L.; Sudhakar, P.; Sun, D.; Tankelevičiūte, E.; Duarte Tonet, M.; Wang, J.; Wang, T.; Wu, S.; Xu, Y.; Zhang, L.; Zysman-Colman, E. The Golden Age of Thermally Activated Delayed Fluorescence Materials: Design and Exploitation. *Chem. Rev.* **2024**, *124* (24), 13736.

(7) Gibson, J.; Monkman, A. P.; Penfold, T. J. The Importance of Vibronic Coupling for Efficient Reverse Intersystem Crossing in Thermally Activated Delayed Fluorescence Molecules. *ChemPhysChem* **2016**, *17*, 2956.

(8) Yang, Z.; Mao, Z.; Xie, Z.; Zhang, Y.; Liu, S.; Zhao, J.; Xu, J.; Chi, Z.; Aldred, M. P. Recent advances in organic thermally activated delayed fluorescence materials. *Chem. Soc. Rev.* **2017**, *46*, 915.

(9) Andruleviciene, V.; Leitonas, K.; Volyniuk, D.; Sini, G.; Grazulevicius, J. V.; Getautis, V. TADF versus TTA emission mechanisms in acridan and carbazole-substituted dibenzo[a,c]-phenazines: Towards triplet harvesting emitters and hosts. *Chem. Eng. J.* **2021**, *417*, No. 127902.

(10) Park, I. S.; Komiyama, H.; Yasuda, T. Pyrimidine-based twisted donor−acceptor delayed fluorescence molecules: a new universal platform for highly efficient blue electroluminescence. *Chem. Sci.* **2017**, *8*, 953.

(11) Komatsu, R.; Sasabe, H.; Kido, J. Recent progress of pyrimidine derivatives for high-performance organic light-emitting devices. *J. Photonics Energy* **2018**, *8* (3), No. 032108.

(12) Achelle, S.; Hodée, M.; Massue, J.; Fihey, A.; Katan, C. Diazine-based thermally activated delayed fluorescence chromophores. *Dyes Pigm.* **2022**, *200*, No. 110157.

(13) Yu, L.; Yang, C. Multipath exciton harvesting in diazine-based luminescent materials and their applications for organic light-emitting diodes. *J. Mater. Chem. C* **2021**, *9*, 17265.

(14) Wong, M. Y.; Zysman-Colman, E. Purely Organic Thermally Activated Delayed Fluorescence Materials for Organic Light-Emitting Diodes. *Adv. Mater.* **2017**, *29*, No. 1605444.

(15) Ohsawa, T.; Sasabe, H.; Watanabe, T.; Nakao, K.; Komatsu, R.; Hayashi, Y.; Hayasaka, Y.; Kido, J. A Series of Imidazo[1,2-f] phenanthridine-Based Sky-Blue TADF Emitters Realizing EQE of over 20%. *Adv. Opt. Mater.* **2019**, *7*, No. 1801282.

(16) Chen, X.; Bagnich, S.; Pollice, R.; Li, B.; Zhu, Y.; Saxena, R.; Yin, Y.; Zhu, W.; Aspuru-Guzik, A.; Zysman-Colman, E.; Köhler, A.; Wang, Y. Unveiling the TADF Emitters with Apparent Negative Singlet-Triplet Gaps: Implications for Exciton Harvesting and OLED Performance. *Adv. Opt. Mater.* **2024**, *12*, No. 2301784.

(17) Dos Santos, P. L.; Chen, D.; Rajamalli, P.; Matulaitis, T.; Cordes, D. B.; Slawin, A. M. Z.; Jacquemin, D.; Zysman-Colman, E.; Samuel, I. D. W. Use of Pyrimidine and Pyrazine Bridges as a Design Strategy To Improve the Performance of Thermally Activated Delayed Fluorescence Organic Light Emitting Diodes. *ACS Appl. Mater. Interfaces* **2019**, *11* (48), 45171.

(18) Hempe, M.; Kukhta, N. A.; Danos, A.; Batsanov, A. S.; Monkman, A. P.; Bryce, M. R. Intramolecular Hydrogen Bonding in Thermally Activated Delayed Fluorescence Emitters: Is There Evidence Beyond Reasonable Doubt? *J. Phys. Chem. Lett.* **2022**, *13* (35), 8221.

(19) Hodée, M.; Moshkina, T. N.; Massue, J.; Fihey, A.; Roisnel, T.; Katan, C.; Nosova, E.; Achelle, S. Prompt and Thermally Activated Delayed Fluorescence of Quinazoline-Based Derivatives: A Joint Experimental and Theoretical Study. *ChemPhotoChem* **2025**, *9*, No. e202400259.

(20) Kohn, W.; Sham, L. J. Self-Consistent Equations Including Exchange and Correlation Effects. *Phys. Rev.* **1965**, *140*, A1133.

(21) Lee, C.-T.; Yang, W.-T.; Parr, R.-G. Development of the Colle-Salvetti correlation-energy formula into a functional of the electron density. *Phys. Rev. B* **1988**, *37*, 785.

(22) Becke, A.-D. Density-functional thermochemistry. III. The role of exact exchange. *J. Chem. Phys.* **1993**, *98*, 5648.

(23) Frisch, M. J.; Trucks, G. W.; Schlegel, H. B.; Scuseria, G. E.; Robb, M. A.; Cheeseman, J. R.; Scalmani, G.; Barone, V.; Petersson, G. A.; Nakatsuji, H.; Li, X.; Caricato, M.; Marenich, A. V.; Bloino, J.; Janesko, B. G.; Gomperts, R.; Mennucci, B.; Hratchian, H. P.; Ortiz, J. V.; Izmaylov, A. F.; Sonnenberg, J. L.; Williams-Young, D.; Ding, F.; Lipparini, F.; Egidi, F.; Goings, J.; Peng, B.; Petrone, A.; Henderson, T.; Ranasinghe, D.; Zakrzewski, V. G.; Gao, J.; Rega, N.; Zheng, G.;

Liang, W.; Hada, M.; Ehara, M.; Toyota, K.; Fukuda, R.; Hasegawa, J.; Ishida, M.; Nakajima, T.; Honda, Y.; Kitao, O.; Nakai, H.; Vreven, T.; Throssell, K.; Montgomery, J. A.; Peralta, J. E.; Ogliaro, F.; Bearpark, M. J.; Heyd, J. J.; Brothers, E. N.; Kudin, K. N.; Staroverov, V. N.; Keith, T. A.; Kobayashi, R.; Normand, J.; Raghavachari, K.; Rendell, A. P.; Burant, J. C.; Iyengar, S. S.; Tomasi, J.; Cossi, M.; Millam, J. M.; Klene, M.; Adamo, C.; Cammi, R.; Ochterski, J. W.; Martin, R. L.; Morokuma, K.; Farkas, O.; Foresman, J. B.; Fox, D. J. *Gaussian 16*; Gaussian, Inc.: Wallingford, CT, 2016.

(24) Liu, H.; Liu, Z.; Li, G.; Huang, H.; Zhou, C.; Wang, Z.; Yang, C. Versatile Direct Cyclization Constructs Spiro-acridan Derivatives for Highly Efficient TADF emitters. *Angew. Chem., Int. Ed.* **2021**, *60*, 12376.

(25) Serevičius, T.; Skaisgiris, R.; Tumkevičius, S.; Dodonova-Vaitkūniene, J.; Juršenas, S. Understanding the temporal dynamics of thermally activated delayed fluorescence in solid hosts. *J. Mater. Chem. C* **2023**, *11*, 12147.

(26) Kreiza, G.; Banevičius, D.; Jovaišaite, J.; Maleckaite, K.; Gudeika, D.; Volyniuk, D.; Gražulevičius, J. V.; Juršenas, S.; Kazlauskas, K. Suppression of benzophenone-induced triplet quenching for enhanced TADF performance. *J. Mater. Chem. C* **2019**, *7*, 11522.

(27) Serevičius, T.; Skaisgiris, R.; Dodonova, J.; Kazlauskas, K.; Juršenas, S.; Tumkevičius, S. Minimization of solid-state conformational disorder in donor−acceptor TADF compounds. *Phys. Chem. Chem. Phys.* **2020**, *22*, 265.

https://doi.org/10.1021/acsaelm.4c02148
ACS Appl. Electron. Mater. XXXX, XXX, XXX−XXX